Published in Journal of Geophysical Research 108(D13): 4374, doi:10.1029/2002JD002646, 2003

Application of a new wind gust parameterization: Multiscale case studies performed with the Canadian regional climate model

Stéphane Goyette
Department of Geosciences, University of Fribourg, Fribourg, Switzerland

Olivier Brasseur
Laboratoire d'étude des Transferts en Hydrologie et Environnement, Domaine Universitaire, Grenoble, France

Martin Beniston
Department of Geosciences, University of Fribourg, Fribourg, Switzerland

Received 12 June 2002; revised 18 December 2002; accepted 12 March 2003; published 1 July 2003.

[1] The implementation of a physically based parameterization scheme for computation of wind gusts in a numerical regional climate model (RCM) is described in this paper. The method is based on an innovative approach proposed by *Brasseur* [2001] that assumes that gusts occurring at the surface result from the deflection of air parcels flowing higher in the boundary layer. Our parameterization scheme is developed so as to use quantities available at each model time step: consequently, the gusts are also computed for each of these time steps. To illustrate the performances of this novel method, gusts simulated for two severe midlatitude windstorms with the Canadian RCM at various resolutions are compared with observed gust speeds. The study is carried out concurrently for the complex terrain of Switzerland and for the smoother topography of Belgium. A preliminary analysis indicates that this parameterization performs equally well over flat and over mountainous regions; it also responds properly in the strengthening as well as the weakening phases of wind storms. The storm-dependent results rely on the model configuration associated with the downscaling procedure, as well as on the accuracy of the simulated flow fields. The model response is dependent on the resolved topography distribution and height and on the types of lower boundary conditions that affect the stability of the boundary layer. The simulated gusts are generally more realistic at higher resolution over the complex topography of Switzerland but are less sensitive to resolution over the flat terrain as in Belgium. On the basis of these two storms, this study also shows that simple scaling coefficients relating gust speeds and resolution are not an appropriate method for addressing such issues. *INDEX TERMS:* 3307 Meteorology and Atmospheric Dynamics: Boundary layer processes; 3379 Meteorology and Atmospheric Dynamics: Turbulence; 3329 Meteorology and Atmospheric Dynamics: Mesoscale meteorology; 3322 Meteorology and Atmospheric Dynamics: Land/atmosphere interactions; *KEYWORDS:* gusts, parameterization, regional climate model, downscaling, turbulence, PBL

Citation: Goyette, S., O. Brasseur, and M. Beniston, Application of a new wind gust parameterization: Multiscale case studies performed with the Canadian regional climate model, *J. Geophys. Res.*, *108*(D13), 4374, doi:10.1029/2002JD002646, 2003.

1. Introduction

[2] It is well recognized that weather and climatic extremes can have serious and damaging impacts on humans, infrastructures, as well as on forests and wildlife [*Kunkel et al.*, 1999; *Meehl et al.*, 2000]. Among the list of extreme events that occurred over the last decade, one can identify intense midlatitude cyclones forming in the north Atlantic. They produce strong mean winds that may be amplified by excessive gusts over various regions in western Europe and the alpine regions (e.g., the wind storms "VIVIAN" 1990 and "LOTHAR" 1999).

[3] There have been worldwide efforts to improve the sampling of gusts [*Beljaars*, 1987], to diagnose and forecast turbulence [*McCann*, 1999] and/or wind gusts with empirical relationships relevant to many applications in weather forecasting, particularly for winds within hurricane [*Jagger et al.*, 2001; *Darling*, 1991]. Other studies focused on high winds in general using model-generated soundings [*Hart and Forbes*, 1999], on the temporal and spatial structure of wind gusts per se [*Mitsuta and Tsukamoto*, 1989] or in

relation with other meteorological quantities [*Davies and Newstein*, 1968; *Endlich and McLean*, 1965], and on the statistical analysis of extreme velocities (overview by *Palutikof et al.* [1999]). There have also been attempts to analyze the change in simulated wind extremes under CO_2 doubling [e.g., *Zwiers and Kharin*, 1998], to statistically model strong winds using various empirical gust factors [*Krayer and Marschall*, 1992; *Weggel*, 1999; *Jungo et al.*, 2002] or to infer wind gust velocities with a physically sound approach using the simulated results from a mesoscale model [*Brasseur*, 2001]. There exists no common physically based parameterization to simulate wind gusts in numerical weather prediction (NWP), nor in regional climate models (RCM), however. In view of the damage potential of gusts, such as those produced by midlatitude synoptic storms, the parameterization of the gustiness of wind requires particular consideration.

[4] In a recent study by *Goyette et al.* [2001], a multiscale analysis of the simulated anemometer-level winds with the Canadian Regional Climate Model (CRCM) has shown that the downscaling of the February 1990 VIVIAN windstorm underestimated the gust velocities. Since gusts are fundamental characteristics of the variability of wind climate, a physically based parameterization to simulate gusts is necessary to better capture the effects of extremes associated with these features. Following the innovative method of *Brasseur* [2001], where the gusty nature of the wind at the surface is diagnosed as the result of the deflection of air parcels generated in turbulent eddies in the boundary layer, a parameterization for use in a numerical model is proposed in this paper. The method includes an estimation of a lower and upper bounds, which provide a confidence interval around the mean wind gust speed. In this study, the parameterization is developed to simulate the most probable estimate of gusts, above a lower bound set to the magnitude of the hourly mean anemometer-level wind speed.

[5] The CRCM serves here as the host model for testing these ideas. This RCM has, on numerous occasions, proven to be a valuable downscaling technique for simulating climate [*Laprise et al.*, 1998] or even shorter-term weather conditions, by allowing physically based and computationally affordable integrations at high spatial resolution. The high spatial resolution is needed both in the horizontal and in the vertical because gust components, that may represent a significant fraction of the wind field, depend on the simulated planetary boundary layer structure as well as on the complexity of the orography.

[6] In this paper, multiscale simulations of gusts are performed and analyzed over Belgium, representative of flat terrain, and Switzerland, representative of complex terrain. The gust speeds simulated with the CRCM at 20, 5, and 1 km grid spacing are compared with station observations. This analysis will thus also allow a direct comparison with previous results presented in *Brasseur* [2001], as well as those obtained by *Goyette et al.* [2001].

[7] A brief description of the CRCM is provided in section 2, followed by a more detailed description of the wind gust parameterization. In sections 3.2 and 3.3 a summary of each of the two windstorms at the synoptic scale is provided, followed by a comparison between the National Centers for Environmental Prediction-National Center for Atmospheric Research (NCEP-NCAR) and the 60-km CRCM flow fields. Subsequently a multiscale comparison of the simulated and observed wind gusts is discussed. In section 4 the possible causes that explain the significance of the simulated wind gusts in terms of daily averages and variances are addressed.

2. Description of the CRCM

2.1. The Atmospheric Model

[8] The current version of the CRCM is the result of the conjoining of a dynamical kernel, MC2, described in *Laprise et al.* [1997] and physical parameterizations that are basically the physics module of the second generation Canadian GCM (hereinafter GCMII), described in *McFarlane et al.* [1992]. The main features of the CRCM are described by *Laprise et al.* [1998] and by *Caya and Laprise* [1999]. In this study, the lateral and uppermost nesting consists of driving the CRCM with a time series of observed atmospheric flow fields, namely pressure, temperature, water vapor and horizontal wind. These driving fields prescribed at the external boundaries are gradually blended with the corresponding ones in CRCM within a "sponge region" of variable width. Prescribed sea surface temperature (SST), sea-ice and other fixed geophysical fields are interpolated onto the CRCM grid at the lower boundary (orography, soil and vegetation types for example). In addition, the CRCM has an option allowing nudging the large-scale flow over the entire domain. This technique called "spectral nesting" [*Biner et al.*, 2000], thus prescribes the evolution of larger scales of the circulation and allows the model to develop its own scales of the flow pattern. The CRCM also has a self-nesting option that allows the flow fields to be simulated at very high resolution in a stepwise manner. The overall nesting procedure is designed to be one-way, that is, there are no feedbacks from the fine scales to the large scales.

[9] CRCM physics involves classical parametric representations of the unresolved subgrid-scale components of the circulation. These include the unresolved radiative and turbulent transfer processes, cloud formation, the generation of precipitation and latent heat release, and also surface energy balance and hydrology. The original GCMII cloud onset function has been modified by *Laprise et al.* [1998] for most current applications with CRCM.

2.2. Description and Parameterization of Wind Gusts in the CRCM Physics

[10] The basics of the method used to compute mean wind gusts follow the wind gust estimates (WGE) of *Brasseur* [2001]. The approach assumes that surface gusts result from the downward deflection of air parcels, flowing higher in the boundary layer, by turbulent eddies. The WGE method takes into account the mean wind and the turbulent structure of the atmosphere. In addition, the method includes the computation of a bounding interval around the gust estimate, which provides a range of likely gust magnitudes.

[11] In the planetary boundary layer (PBL) the turbulent wind field may be regarded as the superposition of a large number of eddies of various sizes, the largest having the transverse dimension of the depth of the PBL, and the smallest being those that are rapidly damped out by friction.

Momentum is thus frequently transported upward and downward. It may happen that under specific conditions, moving air parcels generated within eddies in the PBL are deflected toward the surface, thus producing gusty type of winds. This may be considered as a case where momentum flux is transported from the PBL toward the surface.

[12] Turbulence is characterized by timescales proportional to the life span of eddies, which ranges from few seconds for the smallest to few minutes for the largest. These transient phenomena cannot be explicitly resolved by the mean momentum equations in RCMs and must then be parameterized as subgrid processes. The algorithm adopted to compute the wind gusts implies the knowledge of the turbulence kinetic energy (TKE). TKE is generated by thermal as well as by mechanical processes. It is suppressed within a stably stratified PBL and dissipated as heat by friction. TKE is associated with the generation of eddies within the PBL that may potentially transport momentum from a certain level in the atmosphere down to the surface. It is thus the essential source for gusts close to the surface.

[13] However, the CRCM does not solve explicitly for the turbulence kinetic energy since it has a first-order turbulence closure only. Such a closure computes eddy diffusion coefficients using diagnostic relations, as defined by *McFarlane et al.* [1992]:

$$(K_m, K_h) = l_m^2 \left| \frac{\partial \mathbf{V}_H}{\partial z} \right| [f_m(Ri), f_h(Ri)]. \tag{1}$$

$V_H = [u,\ v]$ is the resolved horizontal wind, f_m and f_h are dimensionless functions of the atmospheric stability taken into account by the local Richardson number, which is defined as

$$Ri = \frac{\frac{g}{\theta}\frac{\partial \theta}{\partial z}}{\left(\frac{\partial V_H}{\partial z}\right)^2}. \tag{2}$$

The master mixing length is defined following *Blackadar* [1962]:

$$l_m = \frac{kz}{1 + \frac{kz}{l_o}}, \tag{3}$$

where l_o, the asymptotic mixing length is fixed at 100 m, and k is the von Kármán constant.

[14] According to its fundamental role in the wind gust estimate method, TKE has to be parameterized as a function of the available model variables. More specifically, the parameterization is based on the "level 2" turbulence second-order closure of *Mellor and Yamada* [1974], whereby an equilibrium is assumed between the shear production terms, the buoyant production or consumption term and a dissipation term. Dissipation of momentum is considered to be proportional to $\mathrm{TKE}^{3/2}/B_1 l_m$ [*Moeng and Sullivan*, 1994; *Mellor and Yamada*, 1982]. Note that the "level 2" model is valid when the time period and spatial dimensions are greater than the life and dimensions of individual eddies that transport momentum and heat. The vertical turbulent fluxes computed in CRCM are expressed in terms of the flux-gradient first-order closure as follows:

$$\overline{s'w'} = K\frac{\partial s}{\partial z}, \tag{4}$$

where $s' = [u',\ v',\ \theta']$ are the turbulent fluctuations of $s = [u,\ v,\ \theta]$, which correspond respectively to the resolved horizontal wind components and to the potential temperature, and $K = [K_m, K_m, K_h]$, are the eddy diffusivities. The diagnostic determination of TKE is then given by

$$TKE = \frac{1}{2}\left\{ B_1 l_m \left[K_h \left| \frac{\partial V_H}{\partial z} \right|^2 (Pr - Ri) \right] \right\}^{2/3}. \tag{5}$$

In equation (5) B_1 is an empirical parameter fixed at 16.6 [*Mellor and Yamada*, 1982], and all other quantities computed at each time step are l_m, the mixing length, Pr, the turbulent Prandtl number defined as K_m/K_h, the ratio of the turbulent transfer coefficients for momentum to that for heat, and the height above the local terrain, z.

[15] A potential problem may arise using equation (5). Turbulent dissipation is always a positive quantity, and difficulties may arise when strong negative buoyancy is greater in magnitude than shear production. However, the hypothesis for using this equation implies that dissipation of TKE is always in equilibrium with the production/destruction terms so that, in other words, TKE is positive whenever $Pr > Ri$.

[16] *Hart and Forbes* [1999] pointed out that the question is not whether midlevel winds are sufficiently strong, but whether boundary layer stability is sufficiently low and vertical wind shear is sufficiently large to allow transport of high-momentum air to the surface as gusts. In line with this assumption, their empirical wind gust probabilities product is replaced in this study with a physically based parameterization for on-line computation of gust speed in a numerical atmospheric model. A step forward is now taken by realizing that the wind shear is the main source of TKE in the PBL. According to *Brasseur* [2001], the deflection of air parcels, inducing the wind gusts at the surface, may be inferred by locally comparing the mean TKE profile with the energy produced by buoyancy forces in the PBL. Gustiness occurs at the surface whenever the mean TKE in a layer is sufficient to overcome the net buoyant energy contained within that layer. The gust speed is thus determined as the wind speed prevalent in the layer if this condition is fulfilled. Taking into account the modification proposed by *Burk and Thompson* [2002], and acknowledged by *Brasseur et al.* [2002], this condition is expressed as

$$\frac{1}{z_p - z'}\int_{z'}^{z_p} TKE(z)dz \quad \geq \quad g\int_{z'}^{z_p} \frac{\Delta\theta_v}{\Theta_v}(z)dz; \qquad 0 \leq z' \leq z_p \ \text{ and } \ z_p \leq z_{PBL}, \tag{6}$$

where z_p is the parcel height, z_{PBL} is the PBL height, g is acceleration due to gravity, $\Delta\theta_v$ is the virtual potential temperature between the environment at height z' and a

parcel adiabatically displaced from z_p down to z', and θ_v the virtual potential temperature at height z_p. Practically, z' may be height chosen between zero and the anemometer level. A parcel at the height z_p is able to reach the anemometer level if the equation (6) is satisfied at all level z' located below z_p.

[17] A first estimation of the boundary layer depth, referred to as h, expressed in terms of a bulk Richardson approach, is computed according to the method of *Troen and Mahrt* [1986]. The idea is based on the use of a specified critical bulk Richardson number, $Ri_{B,cr}$ to infer the mixing height as follows:

$$h = RI_{B,cr}\frac{|V_H(h)|^2}{\frac{g}{\theta_o}[\theta(h)-\theta_o]}, \tag{7}$$

where $V_H(h)$ and $\theta(h)$ are the wind speed and potential temperature at the boundary layer top, and θ_o is the potential temperature at the surface. In most numerical models $Ri_{B,cr}$ giving realistic mixing heights ranges from 0.1 to 1.0 [see, e.g., *Vogelezang and Holtslag*, 1996]; this is due to differences in vertical resolution and parameterization schemes. For the present applications $Ri_{B,cr}$ has been arbitrarily set to 0.25.

[18] To alleviate a problem related to the underestimation of the heat tendency due to the numerical scheme used to solve the vertical diffusion, a procedure finding a boundary layer "top" has been devised [*McFarlane and Laprise*, 1985]. This level, h_{top}, is determined by comparing the heat required bringing the local profile to neutral stability, to the available surface heat flux. Practically, the top of the PBL in the wind gust routine is taken to be the maximum of these two values, that is, $z_{PBL} = \max[h, h_{top}]$.

[19] Many parcels traveling at different heights may have a mean TKE intense enough to overcome the buoyancy forces. The estimated mean wind gust is taken as the maximum wind speed found in the PBL as

$$G = max\left[\sqrt{u^2(z_p)+v^2(z_p)}\right] \tag{8}$$

for every z_p satisfying equation (5). In addition to this mean value, *Brasseur* [2001] proposed a method to compute a lower bound, G_{LB}, to the gust estimate. For our practical use, the lower bound of the gust speed estimate is set to a characteristic wind speed at the anemometer-level. The opportunity is thus taken from the diagnostic computation carried out in this physics package of the anemometer-level wind speed according to similarity theory such that $|V_{anem}| = (u_*/k)\ln(z/z_o)$, where $|V_{anem}|$ is the anemometer wind speed, $u_*^2 = C_M|V_a|^2$, u_* is the friction velocity, C_M is a momentum bulk transfer coefficient, $|V_a| = (u_a^2 + v_a^2)^{1/2}$is the lowest model-level wind speed, z_o is the roughness height for momentum, and z is the height above the surface (typically 10 m).

[20] The method proposed in this paper is qualified as diagnostic and noninteractive, that is, it uses quantities computed by the physics but does not feed back on the flow fields or other model variables. The scheme is implemented so as to be used at each model time step in order to better capture the temporal variability of the gusts.

[21] Implementing such a gust parameterization in a numerical model is interesting for a number of reasons. First, when compared to the "off-line" method of *Brasseur* [2001], that estimates a series of gusts at a temporal resolution corresponding to the archival frequency of particular model outputs, the "on-line" approach described above allows the analysis of a time series of gusts at the temporal resolution corresponding to the model timestep. The off-line method underestimates the gust speeds when these occur between archival times. The on-line method on the other hand captures the rapidly evolving nature of wind. In addition to a better representation of the behavior of simulated gusts in a RCM, this scheme is relevant for the prediction of gusts in a NWP.

3. Model Configurations, Experiments, and Results

[22] In order to evaluate the performance of this wind gust parameterization, two synoptically driven strong wind events, respectively the February 1990 VIVIAN and the December 1999 LOTHAR extra-tropical windstorms, have been simulated at different resolutions with the CRCM, using the self-nesting technique. The driving data used in this investigation, provided by NCEP-NCAR reanalysis [*Kalnay et al.*, 1996] at a spectral T32/L12 resolution, extending from mean sea level to approximately 50 hPa aloft, with an archival period of 12 hours. A synoptic overview between observed and simulated flow fields at 60 km is first provided. Then, multiscale analysis of the simulated gust speeds is carried out. To gain insights on the influence of the complexity of the underlying terrain, we compared model results with observations successively over Swiss mountain stations and over Belgian stations. In Switzerland, the observed wind speeds are compiled every 10 min by MeteoSwiss (the Swiss Meteorological Service), where the data are recorded by the automatic weather station network (ANETZ). The hourly mean is taken as the mean of the 6-hourly values and the gust as the hourly maximum value. In the Belgian data sets the hourly mean is given as the wind averaged over 10-min periods before each hour. Location of Swiss (Nb. 1 to 6) and Belgian stations (Nb. 7 to 9) is shown in Figure 1.

[23] To illustrate concisely the model results, maps of the daily mean wind gusts simulated with the CRCM at 20, 5, and 1 km are shown. The comparison between the observations versus the simulated results over Switzerland and Belgium is carried out in terms of the daily means, which enable assessments to be made as to the ability of the parameterization to capture the magnitude of the gusts. Then, the standard deviations (SD) determine the gusts' variability about the daily mean and the difference between the maximum and the minimum gust values (Max – Min) found during the period under consideration are analyzed. They represent a measure of the amplitude of wind gust speed. Finally, the linear correlation coefficient (r_{o-s}) and the square root of the variance (RMS) quantify the degree of agreement between the observed and the simulated values. In Switzerland, the stations are chosen to illustrate a certain range of response in terms of the variability of gust velocities induced by the behavior of the PBL for different

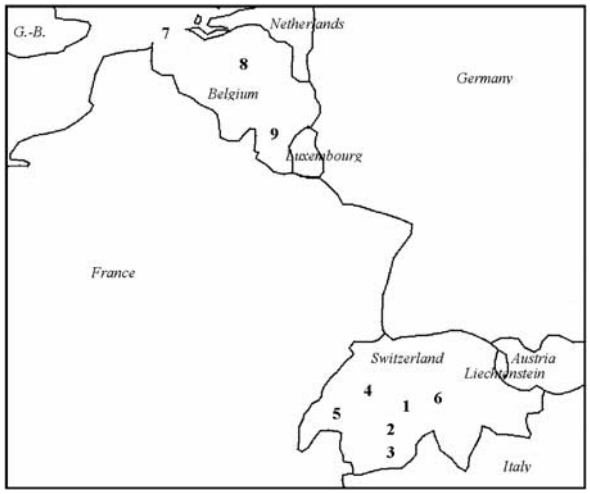

Figure 1. Location of Swiss ANETZ (numbers 1–6) and Belgian synoptic stations (numbers 7–9). Numbers are assigned to stations in Tables 1, 2, and 3.

classes of terrain elevations. In Belgium, the stations are chosen to illustrate a range of response in terms of land-sea transition and distance inland.

3.1. Model Configurations

[24] Details of the model configurations can be found in *Goyette et al* [2001]. The windstorms are simulated on four embedded grids at 60, 20, 5 and 1 km grid spacing, which are referred to domains A, B, C, and D, as shown in Figure 2. Compared with *Goyette et al.* [2001], this study includes an additional 20-km simulation that has been performed in order to analyze the sensitivity of the wind gusts to increasing model resolution. Wind gust speed maximum is saved at hourly intervals. The simulated wind gust speeds are analyzed for the B, C, and D grids over Switzerland and over Belgium. The domain centers of the 1-km grids (D) over southern Switzerland differ slightly in position to each other, in order to better capture the simulated events and to avoid "border" effects related to the model's buffer zone surrounding the computational domain.

[25] The gust parameterization is not tested at 60 km because the topography of the Alps is poorly resolved at this scale and the distributions of the gusts are not accurate. The surface elevation is indeed better represented at resolutions of 20 km and finer; in particular, alpine valleys begin to be adequately represented at horizontal resolutions finer than 5 km. The PBL behavior is also better simulated with increasing vertical resolution, and so are the gust distributions. The spectral nudging technique is used to downscale NCEP-NCAR flow fields at 60 and 20 km with the CRCM on domains A and B respectively. The self-nesting configuration to simulate these events then consists in nesting the simulation at 20 km with 30 vertical levels and an archival period of 3 h in the 60-km simulation; the next step is to nest the 5-km simulation with 30 vertical levels and an archival period of 1 h in the 20-km simulation; the latter finally serves to nest the simulation at 1 km with 46 vertical levels. Subsequently, both events are simulated with the 5-km resolution CRCM driven by the 20-km simulation and 1-km CRCM driven by the 5 km simulation. The vertical level distribution of the 20-km CRCM is basically that of the 5-km one.

3.2. The February 1990 VIVIAN Case

[26] VIVIAN is a remarkable example of intense westerly flow in Europe. It is one of the main flow types during the winter season induced by the more pronounced depression activity to the north of Switzerland during this period [*Swiss Climatological Atlas*, 1995]. The atmospheric conditions observed during the VIVIAN storm have been analyzed by *Schüepp et al.* [1994]. More recently, numerical simulations of this storm have been carried out, along with a multiscale analysis of the simulated fields, by *Goyette et al.* [2001]. During the period 25–28 February an explosive cyclogenesis in the North Atlantic gave rise to severe winds in western Europe that produced damaging gusts over Switzerland. Observations in southern Switzerland show that winds and gusts were particularly strong on 26–27 February as they also were in eastern France, Belgium, and northern Italy. The observed maximum hourly wind gust reached more than 60 m s^{-1} at Jungfraujoch (3580 masl) in the Swiss Alps and 75 m s^{-1} at the Grand St. Bernard (2472 masl) station on the Italian-Swiss border. The NCEP-NCAR and the 60-km simulated synoptic conditions at 1200 on 27 February on the A grid are displayed in Figure 3. The 60-km

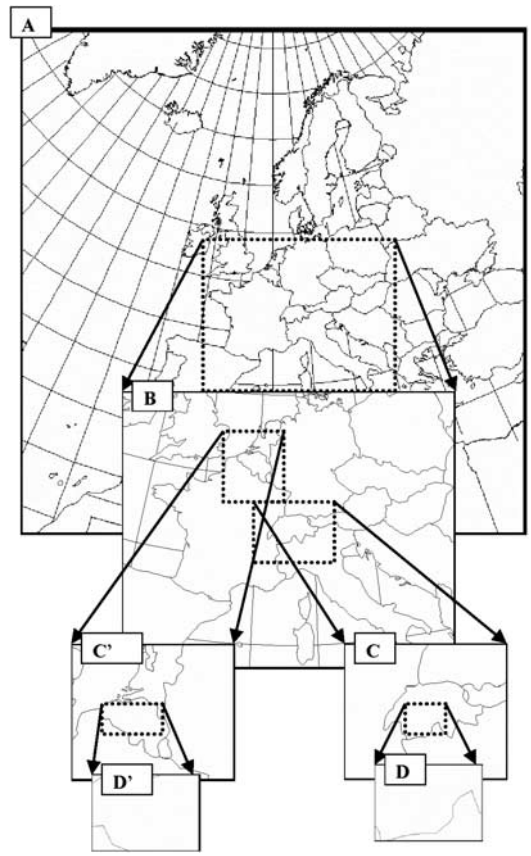

Figure 2. Domains of integration. The outer domain A is used to downscale NCEP-NCAR reanalysis at 60 km. Intermediate domain B is used for the 20-km integrations; domains C and C' are used for 5-km integrations, and domains D and D' for the 1-km integrations.

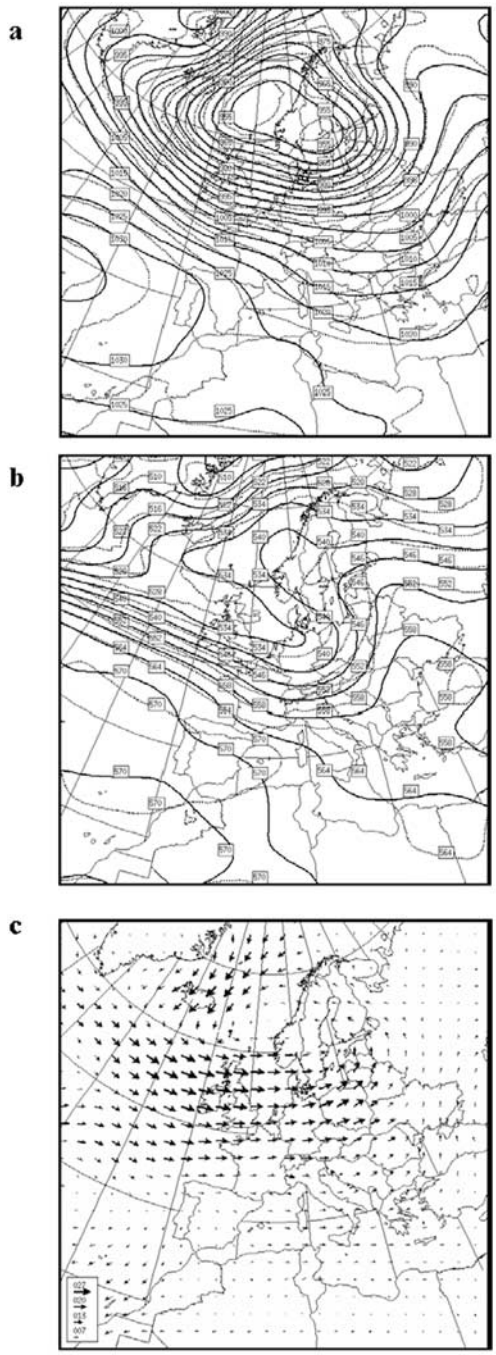

Figure 3. NCEP-NCAR (solid, black) and simulated at 60 km (dotted, gray) mean sea-level pressure (Figure 3a) in hPa, 1000−500 hPa thickness (Figure 3b), and 1000 hPa velocity field (Figure 3c) at 0000 UTC on 27 February 1990 over CRCM domain A. Contour interval for pressure is 5 hPa, that for thickness is 6 dam, and wind speed vectors (m s^{-1}) shown in insert.

simulated mean sea level pressure, the 1000−500 hPa thickness as well as the wind field at 1000 hPa patterns are in agreement to that of the reanalysis data over the computational domain A. Embedded in the powerful westerly jet within the elongated west-east front region, a short baroclinic wave formed in the North Atlantic, deepened west of France to become a secondary depression embedded in the large Scandinavian low VIVIAN and moved east over central Europe. However, NCEP-NCAR as well as the simulated data shows that winds were not intense enough over western Europe, as well as over Belgium and Switzerland (15 to 17 m s^{-1}), to refer to that storm as an ''extreme'' event.

3.2.1. The 20-km Simulation

[27] A spatial distribution of the daily average simulated maximum wind gust during 27 February 1990 in a subdomain of the B grid, centered over Switzerland, is displayed in Figure 4a. Sustained wind gust speeds over 20 m s^{-1} (Beaufort 8, denoting a gale) are found in Switzerland, northern France, Belgium, and western Germany. Daily maximum gusts above 25 m s^{-1} (Beaufort 10, denoting a storm) are found over western southwestern Switzerland and over western Germany. When compared to the hourly mean anemometer-level wind speed field simulated at 60 km, the mean wind gust patterns simulated at 20 km are similar on the large scale, but with enhanced wind velocities. The wind gust parameterization is qualified in the subsequent text as intermittently or fully operative meaning that the simulated wind gust is, respectively, occasionally or constantly greater than the anemometer-level wind during the period under consideration. When the wind gust parameterization is operative, the gust is given by the wind speed simulated on the computational level corresponding to height z_p located 10 m over the resolved surface but lower than z_{PBL}. The gust parameterization is thus operative over Switzerland

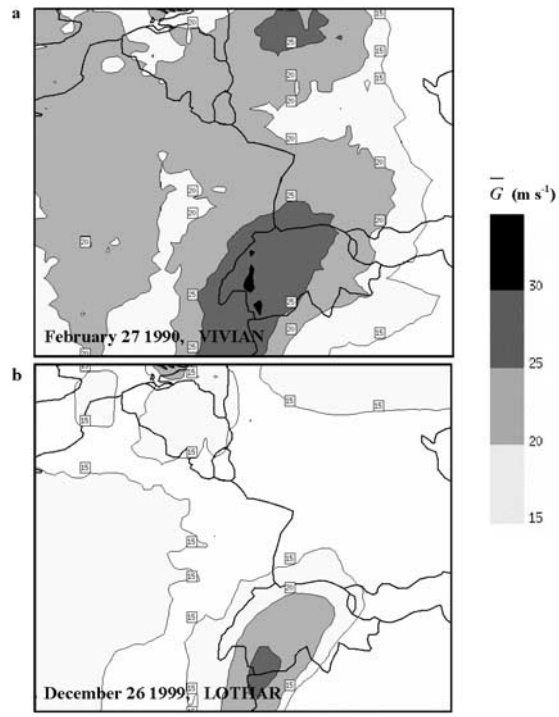

Figure 4. Daily averages of hourly mean windgusts ($\overline{G}$) simulated with the CRCM at 20 km during the two episodes: VIVIAN (Figure 4a) and LOTHAR (Figure 4b). Isotachs are contoured every 5 m s^{-1}, and gray tones start at 15 m s^{-1}.

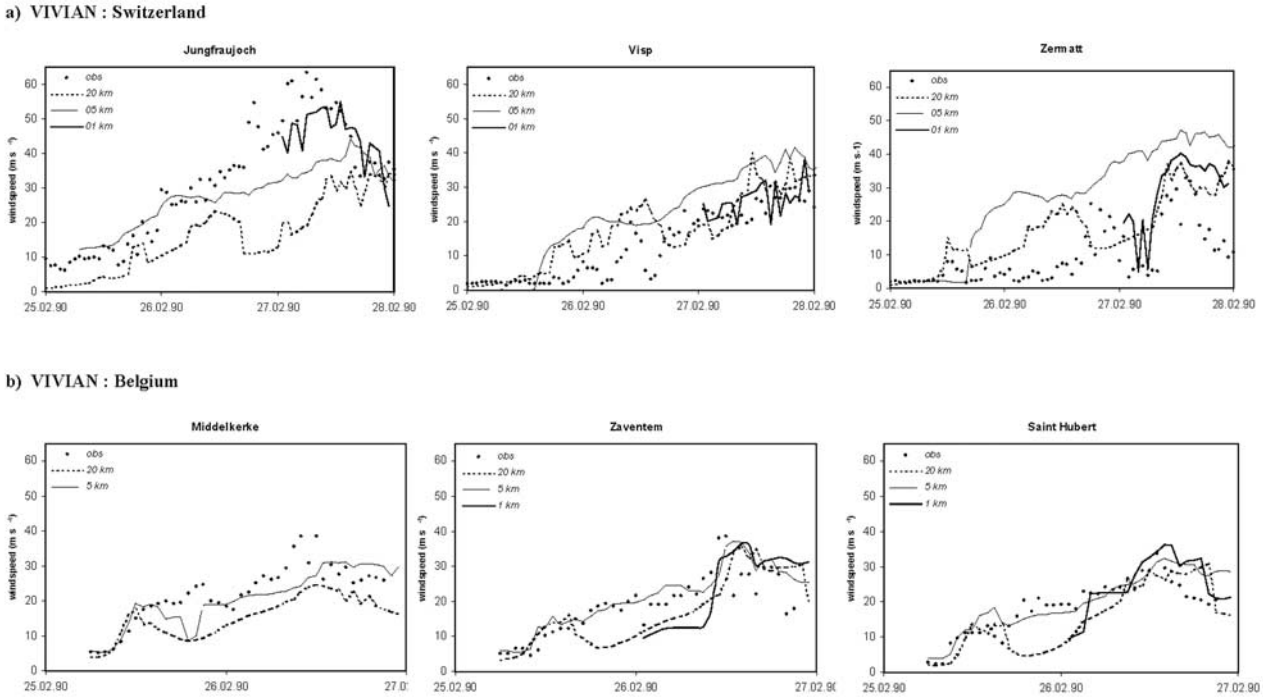

Figure 5. Temporal evolution of the observed and simulated windgusts (m s^{-1}) during 25–28 February 1990 at Swiss ANETZ stations (Figure 5a) and during 25–27 February 1990 at Belgian synoptic stations (Figure 5b).

on 27 February, western Germany during 26–27 February, and Belgium and northern France on 26 February.

[28] The temporal evolution of wind gusts recorded at selected Swiss ANETZ and Belgian synoptic stations, as well as these simulated by the CRCM at 20, 5, and 1 km at grid points located close to the stations during the entire VIVIAN event, is shown in Figure 5. Details concerning the observed and simulated station elevations and gusts statistics are provided in Table 1.

[29] At Visp in the Rhône valley (Canton of Valais, Switzerland), the 20-km CRCM simulates well the remarkable increase in wind gust speeds from 25 to 28 February; it captures the magnitudes of the daily average wind gusts and most of the variability but overestimates the daily amplitude and the daily variability, represented respectively by the difference (Max – Min) and by the standard deviation (SD) in Table 1. The correlation between the simulated and observed gusts is fair (r_{o-s} = 0.50), but the model tends to simulate more temporal variability than observed (SD and RMS = 6.9 m s^{-1}). At the high elevation site of Jungfraujoch in the Canton of Bern, the model simulates the increase in wind gust speeds up to the evening of 26 February but fails to reproduce the very strong winds of 27 February. The simulated gusts matched the observed ones again later in the morning of 28 February. This resulted in an underestimation of the daily mean simulated wind gust speed, of the variability as well as the daily amplitude, and consequently to a high RMS value and to a poor correlation coefficient. At Zermatt (Canton of Valais), the model simulates the increase in wind gust speeds up to the evening of 26 February too rapidly but succeeds in reproducing the stronger winds of 27 February. The simulated winds of 28 February exceed the observed ones, however. This resulted in an overestimation of the daily mean simulated wind gust speed and to lower standard deviation and daily amplitude. The correlation coefficient is reasonable but the RMS value is not negligible implying that differences exist between observed and simulated hourly means.

[30] At Middelkerke on the coast of the North Sea in Belgium, the 20-km CRCM simulates well the increase in wind gust speed from late 25 February to the night of 26 February. It captures the magnitudes of the daily average wind gusts but overestimates slightly their variability. It also captures well the daily amplitude and the daily variability, represented respectively by the difference (Max – Min) and by the SD values in Table 1. The correlation between the simulated and observed gusts is weak (r_{o-s} = 0.34) and the model tends to simulate more temporal variability compared to the observations (RMS = 8.6 m s^{-1}). At the Saint Hubert station located in the southeastern part of Belgium, the observed increase in gust speed is underestimated late on 25 February, but the peak gusts during late 26 February are reasonably well captured. This resulted in a slight underestimation of the simulated wind gust velocity and an overestimation of the temporal variability and of the daily amplitude. The correlation between the simulated and observed gusts is good (r_{o-s} = 0.47) but the model tends to simulate more temporal variability compared to the observations (RMS = 6.6 m s^{-1}). At Zaventem in central Belgium the observed increase in gust speed during 26 February is underestimated. This resulted in an overall underestimation of the simulated wind gust speed and an underestimation of the temporal variability and of the daily amplitude. The correlation between the simulated and

Table 1. Station Elevations and Daily Statistics of Observed and Simulated Wind Gusts in Switzerland and Belgium for VIVIAN Storm[a]

Station Name and Number[b]	Grid	Elevation, m	Daily Mean Gust, m s^{-1}	Standard Deviation, m s^{-1}	RMS,[c] m s^{-1}	r_{o-s}	Max – Min, m s^{-1}
			Switzerland, 27 February 1990				
Jungfraujoch (1)	observed	3580	48.1	10.3	–	–	30.8
	20	1392	27.3	6.0	25.4	−0.57	18.4
	5	2595	36.9	3.2	16.2	−0.33	12.1
	1	3153	45.0	7.5	8.6	0.63	30.2
Visp (2)	observed	640	24.1	3.5	–	–	11.3
	20	1412	27.6	6.9	6.9	0.50	24.5
	5	2034	35.6	3.6	11.9	0.60	11.2
	1	1091	26.3	4.6	5.1	0.37	19.2
Zermatt (3)	observed	1638	16.1	9.4	–	–	29.5
	20	1467	26.9	7.9	13.1	0.65	23.7
	5	2696	43.3	2.7	28.4	0.58	9.2
	1	2320	29.6	10.0	15.4	0.70	35.3
			Belgium, 26 February 1990				
Middelkerke (7)	observed	4	27.4	5.2	–	–	21.1
	20	3	19.5	3.4	8.7	0.74	11.7
	5	0	25.9	4.3	5.8	0.32	12.2
	1	–	–	–	–	–	–
Zaventem (8)	observed	55	24.3	6.2	–	–	25.3
	20	76	22.8	8.3	8.6	0.34	25.2
	5	30	27.2	5.2	6.4	0.51	17.5
	1	25	23.1	10.3	8.6	0.48	26.9
Saint Hubert (9)	observed	563	23.7	3.9	–	–	15.8
	20	219	21.9	7.1	6.6	0.47	23.4
	5	345	25.4	4.9	4.7	0.52	15.3
	1	354	25.3	7.5	4.5	0.78	26.9

[a]Daily mean is the arithmetical mean of hourly mean gusts over a complete diurnal cycle; the standard deviation is computed as the root mean square of the average square of the hourly mean gust deviations about the daily mean; the RMS value is computed as the average square of the deviations between the observed and the simulated hourly mean gusts; the linear correlation coefficient (r_{o-s}) represents the degree of common variation between the daily series of observed and simulated hourly mean gusts; and the daily amplitude (Max – Min) is computed as the daily maximum minus the daily minimum found in the series. Station numbers are illustrated in Figure 1.

[b]Numbers in parentheses correspond to those in Figure 1.

[c]Observed minus simulated.

observed gusts is good (r_{o-s} = 0.74) but the model tends to simulate more temporal variability compared to the observations (RMS = 8.7 m s^{-1}).

3.2.2. The 5-km Simulation

[31] A spatial distribution of the daily average simulated maximum wind gust during 27 February 1990 over Switzerland and over Belgium during 26 February 1990 are displayed in Figures 6a and 6b and in Figure 7 respectively on the C grids. Sustained wind gusts of over 35 m s^{-1} (Beaufort 12, denoting hurricane-force winds) are found in Switzerland. This simulated gust pattern is in accordance with the observed one as displayed in *Jungo et al.* [2002]. When compared to the 20-km simulation, the 5 km daily average gust distribution is more detailed, owing to the better-resolved topography. The daily average wind gust speeds also increased markedly over the entire Swiss territory. Daily average wind gusts over 35 m s^{-1} are found along most of the Alps, and gustspeeds over 40 m s^{-1} over higher summits on the borders between France and Switzerland, and Italy and Switzerland. The gust parameterization is particularly operative over the Swiss Alps as well as over the upper Rhône valley, where the gust speeds exceed the hourly mean wind speed by more than 25 m s^{-1} during peak hours of 27 February.

[32] In Belgium, sustained wind gust speeds over 25 m s^{-1} (Beaufort 10) are simulated with maxima exceeding 27.5 m s^{-1} over the eastern part of the country. Daily average wind gusts over 30 m s^{-1} (Beaufort 11, denoting a violent storm) are also found over western Germany. When compared with the 20-km simulation, the 5 km daily average gust distribution is similar, but the gust speeds increased notably by 6 m s^{-1} throughout Belgium and western Germany. The gust parameterization is particularly operative over eastern Belgium and western Germany where the gust speeds exceed the hourly mean wind speed by more than 20 m s^{-1} for a number of hours on 26 February.

[33] The temporal evolution of simulated wind gusts at 5 km grid spacing at Swiss and Belgian stations is illustrated in Figures 5a and 5b, respectively, and details concerning gusts statistics are provided in Table 1. The 5-km CRCM produced generally stronger gusts and weaker standard deviation than the 20-km CRCM. In many cases, the 5-km CRCM also produced weaker RMS values such as those at Belgian stations or at the Jungfraujoch in the Swiss Alps, implying that the simulated gusts are closer to the observed ones. The correlation between observed and simulated gusts often improved compared with the 20-km CRCM. The daily amplitude of simulated gust speeds improved at some Swiss (e.g., Visp) and Belgian stations (e.g., Middelkerke and Saint Hubert). The overall improvement of the 5-km CRCM is notable, both in terms of spatial average as well as in terms of the timing of local gust distributions.

3.2.3. The 1-km Simulation

[34] A spatial distribution of the daily average simulated maximum wind gust during 27 February 1990 over

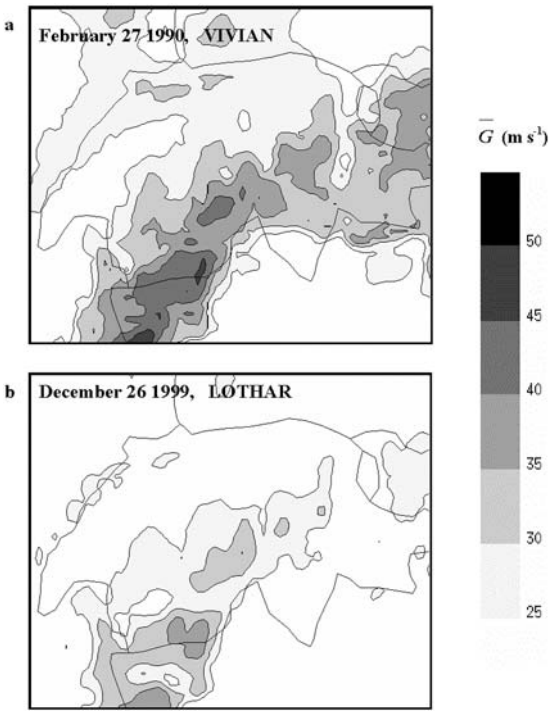

Figure 6. Daily averages of hourly mean windgusts ($\overline{G}$) simulated with the CRCM at 5 km over Switzerland during the two episodes: VIVIAN (Figure 6a) and LOTHAR (Figure 6b). Isotachs are contoured every 5 m s^{-1}, and gray tones start at 25 m s^{-1}.

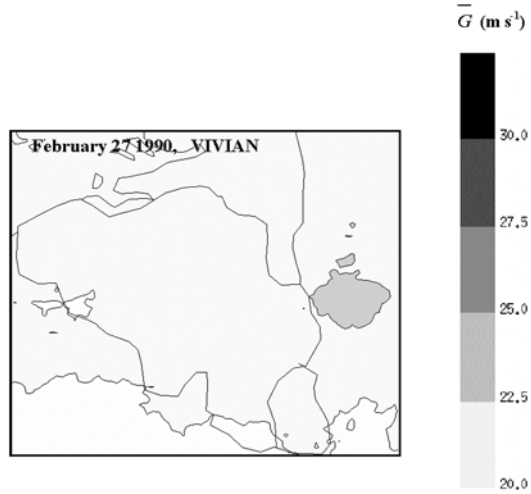

Figure 7. Daily averages of hourly mean windgusts ($\overline{G}$) simulated with the CRCM at 5 km over Belgium during the VIVIAN storm. Isotachs are contoured every 5 m s^{-1}, and gray tones start at 20 m s^{-1}.

southern Switzerland on grid C is displayed in Figure 8a. Sustained wind gusts over 25 m s^{-1} (Beaufort 10) are found distinctly in the southern Alps at the Swiss-Italian border, in the Canton of Valais, and in the Bernese Alps during that particular day with maximum up to 45 m s^{-1} over higher alpine summits. When compared to the 5-km simulation, the 1 km daily average gust distribution is more detailed. Average gust speeds also markedly increased locally, particularly in the Canton of Valais, which is clearly better resolved with a 1 km grid spacing. The gust parameterization is particularly operative over the NW facing slopes of Alpine foothills as well as some of parts the Rhône Valley where the gust speeds exceed the hourly mean wind speed by more than 25 m s^{-1} on 27 February.

[35] The spatial distribution of the daily average simulated maximum wind gust during 26 February 1990 over Belgium (not shown) is characterized by sustained wind gusts ranging from 20 m s^{-1} in the south to more than 24.5 m s^{-1} over the northeastern part of the country. The gust parameterization is operative over the whole domain after 1000 UTC on average, where the gust speeds are often 15 m s^{-1} higher than the hourly mean.

[36] The temporal evolution of simulated wind gusts at 1 km grid spacing at Swiss and Belgian stations is illustrated in Figures 5a and 5b, respectively, and details concerning gust statistics are provided in Table 1. The 1-km CRCM produced daily mean gust speeds that are closer to the observed daily averages, although some differences remained. There is a slight underestimation of 3.1 m s^{-1} and of 1.2 m s^{-1} at Zaventem and an overestimation of 2.2 m s^{-1} at Visp and of more than 13 m s^{-1} at Zermatt. The standard deviations and daily amplitudes are generally closer to the observed ones. The linear correlation coefficients are generally satisfactory, and there is considerable improvement at the Jungfraujoch station when compared with the 20 km and the 5 km CRCM simulations. The RMS values improved (i.e., decreased), but not necessarily linearly, with increasing resolution at Jungfraujoch, Visp, and Zaventem.

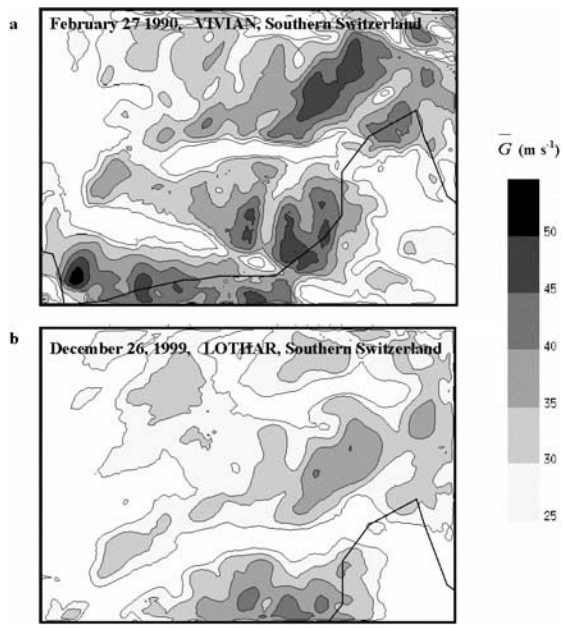

Figure 8. Daily averages of hourly mean windgusts ($\overline{G}$) simulated with the CRCM at 1 km over southern Switzerland during the two episodes: VIVIAN (Figure 8a) and LOTHAR (Figure 8b). Isotachs are contoured every 5 m s^{-1}, and gray tones start at 25 m s^{-1}.

[37] The reasons explaining this improvement in the representation of gusts will be discussed in section 4.

3.3. The December 1999 LOTHAR Case

[38] The December 1999 LOTHAR storm is another example of westerly flow induced by midlatitudes winter cyclones over the northern Atlantic. Some dynamical aspects of this storm are presented by *Wernli et al.* [2002]. On 25 December low-pressure centers deepened to <950 hPa in the North Sea and Norwegian Sea west of Bergen (Norway) at 1200 UTC. An intense jet stream oriented west-to-east, extending from the east coast of North America to Germany crossed a strong baroclinic zone at more than 95 m s^{-1} above the North Atlantic Ocean. On 26 December at 0000 UTC a short baroclinic wave deepened just in front of the jet stream maximum. The severity of the subsequent events arose from the sustained high wind speeds over a wide geographical area, in addition to precipitation that caused a large amount of additional damage. LOTHAR resulted in wind speeds over 58 m s^{-1} in Brittany, France, decayed to 45 m s^{-1} and peaked in the German Black Forest area and in the foothills of the Swiss Alps at more than 65 m s^{-1}. A few hours later, and hundreds of kilometers from the coast, a second storm called MARTIN caused large damage with gusts of 40 m s^{-1} in Piemont and Sicily, as well as considerable flooding in southwestern France and avalanches throughout the alpine chain.

[39] The NCEP-NCAR and simulated synoptic conditions at 0600 UTC on 26 December 1999 at 60 km are illustrated in Figure 9. The 60 km simulated mean sea level pressure, the 1000–500 hPa thickness as well as the wind field at 1000 hPa are similar to that of the reanalysis data over the computational domain A. Although differences exist locally between observed and simulated mean sea level pressure fields, representing 3–4 hPa, the isallobaric fields show a general agreement regarding the short wave trajectory and intensity. On 26 December the short baroclinic wave moved from the coast of Brittany at 0000 UTC to the border between Germany and the Czech Republic at 1200 UTC. The horizontal gradient of the pressure drop over consecutive 6-hour period are −21 and −20 hPa 6 h^{-1} for the observed and simulated mean sea level from 0000 to 0600 UTC, and −27 hPa 6 h^{-1} for both the observation and simulated pressure from 0600 to 1200 UTC. The position and intensity of the simulated jet stream is also generally well reproduced compared to observations. The 1000-hPa winds tend to be similar to the reanalysis data on the average, apart from some localized areas, particularly over the Alps, where differences tend to be greater. Again, NCEP-NCAR as well as the simulated data at 60 km shows that winds were not intense enough over western Europe, and over Switzerland in particular, to refer to that storm as an "extreme" event.

3.3.1. The 20-km Simulation

[40] Unlike the station analysis done in the case of the VIVIAN storm, only the salient features of this storm will be described here.

[41] A spatial distribution of the daily average simulated maximum wind gust during 26 December 1999 over western Europe (subset of computational domain B) is displayed in Figure 4b. Sustained intense wind gusts over 25 m s^{-1} (Beaufort 10) are mainly found in central and southwestern Switzerland and in the Netherlands near the cost of the North Sea. Moderate winds are also simulated in the Black Forest in southern Germany, in northern Germany, and over a west to east strip in northern France where average speeds during that day reached 17–19 m s^{-1}

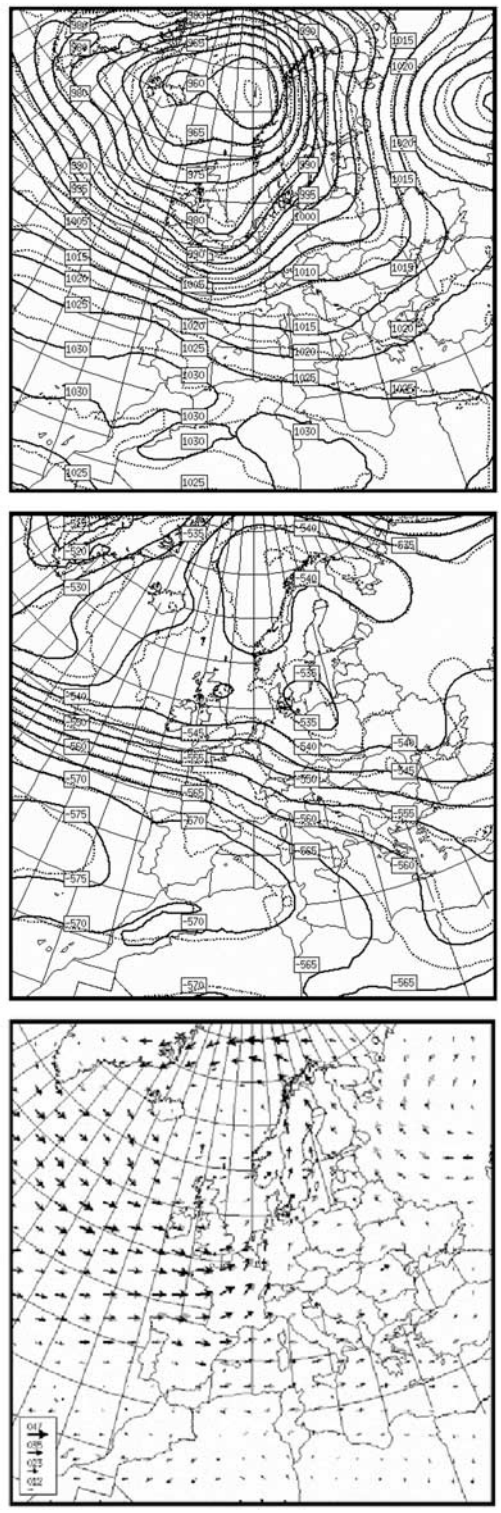

Figure 9. As in Figure 2 but for the 26 December 1999 period.

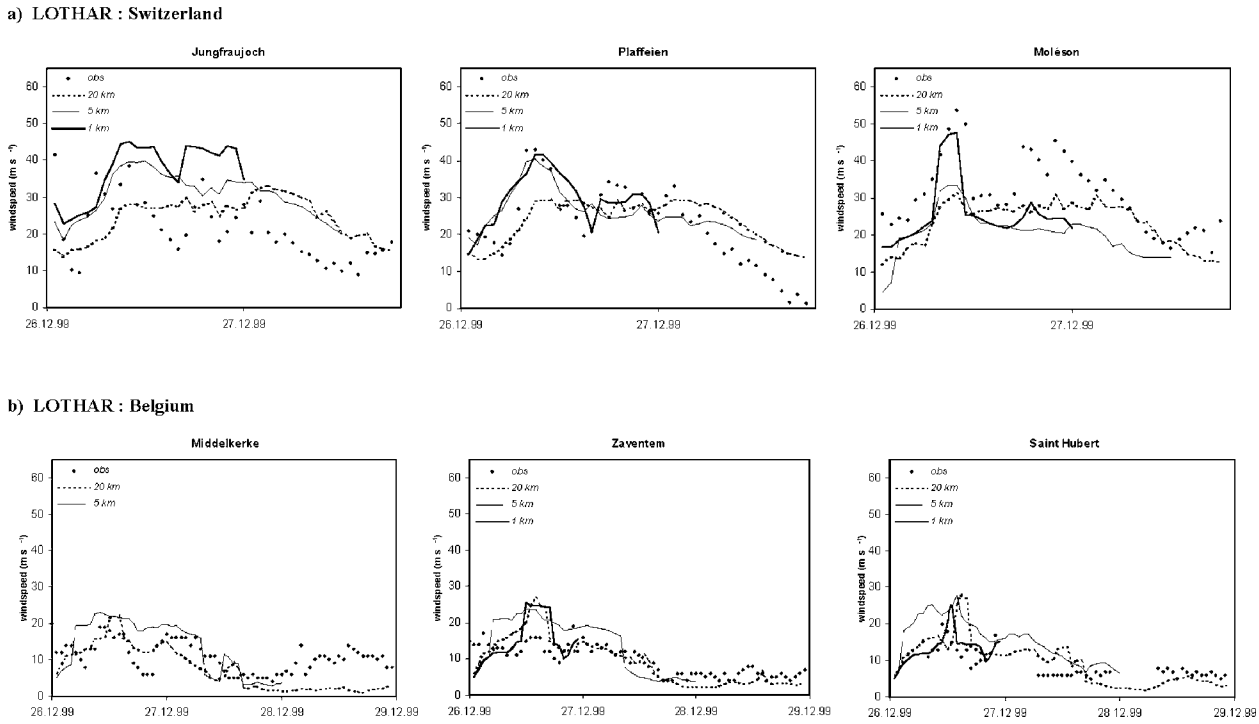

Figure 10. As in Figure 4 but for LOTHAR storm.

(Beaufort 8, denoting a gale). The gust parameterization is fully operative on 26 December over Switzerland where the gust speeds exceed the hourly mean wind speed by 10 m s^{-1} on average. In northwestern Germany and northern France, the gust parameterization is partially operative during this day.

[42] The temporal evolution of wind gusts recorded at selected Swiss ANETZ and Belgian synoptic stations as well as those simulated by the CRCM at 20, 5, and 1 km at grid points located close to the observing stations during 26–29 December 1999 is shown in Figure 10. Details concerning the observed and simulated station elevations and gusts statistics are provided in Table 2.

[43] The gust speeds are generally well reproduced during the strengthening and the weakening phase at Swiss stations, although some intense bursts are not accurately captured on 26 December. The correlation between the simulated and observed gusts is rather good on average but the model tends to simulate less temporal variability compared to the observations.

[44] Belgium is much less affected by the LOTHAR storm than Switzerland. Nevertheless, it is also interesting to assess the behavior of the wind gust estimate method for less extreme events. The transition between strong and weak gusts speeds of 27–28 December is well captured. The daily average of the simulated wind gust speed is slightly overestimated as well as the daily variability and the correlation between hourly winds and gusts is low.

3.3.2. The 5-km Simulation

[45] The spatial distribution of the daily average simulated maximum wind gust during 27 February 1990 over Switzerland is displayed in Figure 6b. Sustained gusts over 35 m s^{-1} are found over southern Alps in Switzerland. Violent gusts over 30 m s^{-1} are also found in the Jungfrau region and gusts over 25 m s^{-1} found along the Swiss Alps as well as over the alpine foothills. This simulated gust pattern is in accordance with the observed one discussed by *Jungo et al.* [2002]. Here again, the gust parameterization is fully operative on 26 December over the Swiss Alps where the gust speeds exceed the hourly mean wind speed by 10 m s^{-1} on average.

[46] In Belgium, winds were not as strong as for the VIVIAN storm. The daily average simulated maximum gusts are roughly 17 to 19 m s^{-1} throughout the country. Therefore a spatial distribution of the daily average gusts is not shown.

[47] The temporal evolution of simulated wind gusts at 5 km grid spacing at Swiss and Belgian stations is illustrated respectively in Figures 10a and 10b, and details concerning gust statistics are provided in Table 2. The 5-km CRCM produced generally stronger gusts and weaker standard deviations than the 20-km CRCM except at the Moléson station, where it decreased by 2.2 m s^{-1} on average during 26 December 1999 and also at Belgian stations where the daily average gust speed increased by about 4 m s^{-1}. The weakening phase in gust speeds from 26 December onward toward weaker values is also reasonably well captured.

3.3.3. The 1-km Simulation

[48] The spatial distribution of the daily average simulated maximum over southwestern Switzerland during 26 February 1990 is displayed in Figure 8b on the C grid. Sustained wind gusts over 25 m s^{-1} (Beaufort 10) are found in the Swiss foothills, particularly in the Cantons of Vaud, Fribourg and Bern, as well as in the prealpine regions. Maxima of up to 40 m s^{-1} are simulated over higher alpine

Table 2. Same as Table 1 but for LOTHAR Storm

Station Name and Number	Grid	Elevation, m	Daily Mean Gust, m s^{-1}	Standard Deviation, m s^{-1}	RMS, m s^{-1}	r_{o-s}	Max – Min, m s^{-1}
			Switzerland, 26 December 1999				
Jungfraujoch (1)	observed	3580	25.2	8.1	–	–	32.1
	20	1392	24.0	5.1	9.15	0.11	16.4
	5	2595	32.0	6.0	11.2	0.22	21.5
	1	3153	37.2	7.5	15.2	0.27	22.3
Plaffeien (4)	observed	1042	27.7	8.0	–	–	28.7
	20	1199	24.3	5.6	7.1	0.62	16.0
	5	933	28.1	6.0	6.0	0.67	23.1
	1	938	29.6	6.9	6.3	0.70	27.0
Moléson (5)	observed	1972	35.7	8.8	–	–	30.9
	20	1222	24.3	5.6	12.9	0.73	19.3
	5	587	22.1	6.4	15.1	0.67	28.9
	1	1199	25.7	8.3	11.8	0.72	30.9
			Belgium, 25 December 1999				
Middelkerke (7)	observed	4	12.8	4.0	–	–	13.0
	20	3	14.1	3.7	3.9	0.55	15.9
	5	0	18.1	5.1	7.9	0.20	17.8
	1	–	–	–	–	–	–
Zaventem (8)	observed	55	13.5	2.3	–	–	10.0
	20	76	15.9	5.0	5.8	0.12	20.6
	5	30	18.7	5.0	7.8	−0.16	18.5
	1	25	15.2	6.2	7.1	0.17	20.5
Saint Hubert (9)	observed	563	13.0	3.2	–	–	12.0
	20	203	14.5	5.3	8.7	−0.06	22.5
	5	345	19.4	5.1	12.3	0.22	21.9
	1	354	13.2	3.9	–	–	19.8

summits. The gust parameterization is particularly operative over the Cantons of Vaud, Fribourg and Bern on the Swiss Mittelland as well as over the prealpine foothills where the gust speeds exceed the hourly mean wind speed by more than 19 m s^{-1} during 26 December.

[49] In Belgium the gust parameterization is particularly operative in the east between 1100 and 1900 UTC on average, where the gust speeds are significant. In eastern Belgium the differences between the hourly gust and the hourly mean is negligible, whereas it reaches more than 10 m s^{-1} in western Belgium.

[50] The temporal evolution of simulated wind gusts at 1 km grid spacing at Swiss and Belgian stations is illustrated respectively in Figures 10a and 10b, and details concerning gust statistics are provided in Table 2. The 1-km CRCM produced daily mean gust speeds that overestimated the observed ones at Jungfraujoch. At Plaffeien, the 1-km CRCM improved the conditions by producing gusts statistics remarkably close to the observations. At the Moléson station, although the daily mean gust speed is lower than observed, the 1-km CRCM captured well one of the gust bursts of 26 December but missed the second one. At the Belgian station Zaventem, the 1-km CRCM reproduced reasonably well the weaker gusts of 26 December, but the daily amplitude is doubled relative to the observations.

4. Discussion

[51] A preliminary analysis is undertaken in order to determine the conditions for which the wind gust parameterization implemented in the CRCM succeed or failed in reproducing the observed gust values. Generally speaking, the wind gust parameterization produced fairly realistic results compared to the observed gust speeds. The accuracy of the simulated gusts, assessed using basic statistics, has shown that mean turbulence kinetic energy compared to the stability within atmospheric layers is a relevant measure to simulate the gusty nature of the winds. As it has been seen above, each storm has a specific signature in terms of spatial gust speed patterns and temporal variations. Given these, it can be readily seen from Figure 4 that the influence of the alpine chain is predominant. The performance of this wind gust parameterization depends not only on the original approach used to infer the gust speeds, but also on the ability of the model to simulate the atmospheric flow fields as well as other relevant quantities. The performance is indeed related to the validation phase where many aspects of the method has already been assessed in *Brasseur* [2001]; in addition, it is also related to the ability of the model to reproduce the synoptic and the mesoscale conditions, and subsequently the PBL behavior simulated during the self-nesting sequences prevailing before and during these windstorms. As shown in the previous studies of *Goyette et al.* [2001] and *Brasseur et al.* [2001], as well as in many other studies with RCMs, the model flow fields may differ with respect to the driving fields (e.g., NCEP-NCAR, ECMWF) but this aspect, while worth mentioning, involves a deeper investigation that lies beyond the scope of the present study. The CRCM self-nesting option employed to downscale reanalysis data has been arbitrarily ''tuned'' to give realistic results, therefore no further effort has been spent to obtain optimal flow fields with increasing resolution.

[52] The wind gust is operative only where the gust speed exceeds the hourly mean wind speed on hourly average. Otherwise, when the TKE is not large enough to overcome the buoyant energy in a layer above the surface, the CRCM anemometer-level wind magnitude is prescribed. To help in interpreting the coherence of the results, site-specific TKE,

z_{PBL}, and wind profiles, $V_H(z)$, are considered. In addition, the ability of the CRCM in reproducing wind gusts may be demonstrated by comparing daily mean and variability of the difference between hourly gusts and hourly mean winds ($\overline{G} - \overline{V}_{anem}$) during the two cases.

4.1. Resolution Dependency

[53] As mentioned by *Goyette et al.* [2001], the simulated anemometer-level wind speed in Switzerland has shown to be sensitive to the resolved "station" elevation during the VIVIAN storm. Here, generally, the simulated wind gust velocities are closer to the observed ones when the grid mesh is finer, owing to the enhanced vertical layer spacing, beginning at 30 levels at 20 and 5 km and reaching 46 at 1 km horizontal grid spacing, and to the better representation of topography. This behavior can be partly explained by the better-resolved TKE and wind profiles, as shown at station Visp in Figure 11, for example. A low-level jet, that is absent in the 20-km simulation, is well captured with the 1-km CRCM, reaching more than 34 m s^{-1} at 1200 UTC on 27 February 1990. If we examine the time series of the gustspeed at Visp in Figure 5, we notice that $\overline{G}$ decreased from 38 m s^{-1} in the 20-km CRCM to 29 m s^{-1} at 1200 UTC in the 1-km CRCM, closer to the observed value of 27 m s^{-1}. This is explained by the wind velocity profile in the PBL. The latter being statically stable also has fairly large TKE values. The simulated PBL height, z_{PBL}, decreased from 2325 m (14th level in the vertical) in the 20 km CRCM to 1278 m (8th level) in the 1-km CRCM. The TKE values, which are significant in the lowest layers of the 20-km CRCM, tend to increase in the 1-km CRCM. At 1200 UTC three regions of strong TKE are found in the PBL, the maximum of 2.9 m^2 s^{-2} found at 1000 m above the surface corresponds to the height below which the gust extracts its energy. It can be seen in Figure 11 that while the wind gust parameterization was operating intermittently in the 20-km CRCM it was fully operative in the 1-km CRCM; this change in behavior is due to the simulated TKE being resolved more strongly in the 1-km simulation and was subsequently able to overcome the strong stability forces that do not change significantly when resolution is increased. Even if the daily mean of simulated gust speed is in relatively good agreement with the observed one, the time evolution of gust speed shows an irregular pattern in time that may not always fit the observed one.

4.2. Influence of the Representation of Turbulence

[54] The value of the linear correlation coefficient may be a poor indicator of the gust activity in this context. As explained in most documents dealing with the boundary layer (e.g., *Stull* [1988]; chapter 1), statically stable air tends to suppress turbulence while the developing low-level jet enhances the wind shear that tends to generate turbulence. This results in intermittent bursts that explain the gusty nature of the wind at the surface. Rapid variation in the value of the simulated TKE with time can be associated with variation in gust speed. In this parameterization the gusts are not modeled as such; they are only embodied by "noninteracting" entities having their speeds determined by equation (8) whenever equation (6) is satisfied in the PBL. A measure of the efficiency of the parameterization may otherwise be given by the difference between the hourly gust and the anemometer-level wind speed. Recalling that the lower bound of the gust speed is prescribed to the anemometer-level wind magnitude, V_{anem}, these differences characterize the effectiveness of the turbulent eddies acting against buoyancy forces. As depicted in Table 3 and in Figure 11, there is a better general agreement between the simulated and observed differences when the model resolution is enhanced and therefore when the TKE above the surface is increased. The means and standard deviations of the difference are generally closer to those observed for the 1-km CRCM than for the 20-km CRCM at most of Swiss and Belgian locations.

[55] The downscaling of reanalysis data at 60 km, to 20 km, to 5 km, and finally to 1 km grid spacing has significantly improved the representation of physical processes such as dynamics, convection, and turbulence, as well as the representation of surface characteristics. The transition from 20 to 46 vertical levels, respectively, improved the representation of the PBL allowing an improvement in the resolution of low-level jets. During the simulated storms, when the condition expressed by the equation (6) is satisfied, the gust speeds can reach much stronger values as a result of the better-resolved low-level jets that are simulated when the CRCM vertical grid spacing is refined. Even if the simulated "average" wind gust speed underestimates the observed one, it may be considered that an "upper bound" of the gust speed is assigned to the fastest winds found in the PBL [e.g., *Brasseur*, 2001]; this would help capturing a number of events, on an hourly basis, at the Swiss station Moléson during the LOTHAR storm, for example, and at station Jungfraujoch during the VIVIAN storm. As previously shown by *Goyette et al.* [2001], the simulated "hourly average" wind gust speeds underestimated the observed ones during the VIVIAN storm in Switzerland. The wind gust parameterization implemented in the CRCM helped to capture the severe gusts recorded at many stations in Switzerland during the VIVIAN storm, considering that the daily mean of $\overline{G} - \overline{V}_{anem}$ reaches significant magnitudes.

[56] When compared to the original WGE results during the period of 26 February 1990 [*Brasseur*, 2001; Figure 18], the CRCM "on-line" mean gust parameterization gives overall similar mean gusts over Belgium but simulates a slightly larger RMS values during that day over the Zaventem, Middelkerke, and Saint Hubert stations. However, the "on-line" method allows for rapidly evolving gusts to be better captured since it is applied at each time steps, while the "off-line" method is constrained by archival intervals of 3 to 6 hours.

[57] Despite the relative success of this parameterization in reproducing severe winds, it appears that at some occasions the simulated winds failed to reproduce gust observations: it occasionally underestimates the stronger gusts (e.g., 1-km CRCM, station Moléson during the LOTHAR storm at 1800 UTC, or station Jungfraujoch during the VIVIAN storm at 0600 UTC). During these episodes, the simulated TKE was not strong enough to overcome the strong static stability of the atmosphere.

[58] Keeping in mind that the reproduction of individual eddies is not expected nor envisaged, this parametric scheme captured the strengthening phase of the gust speed,

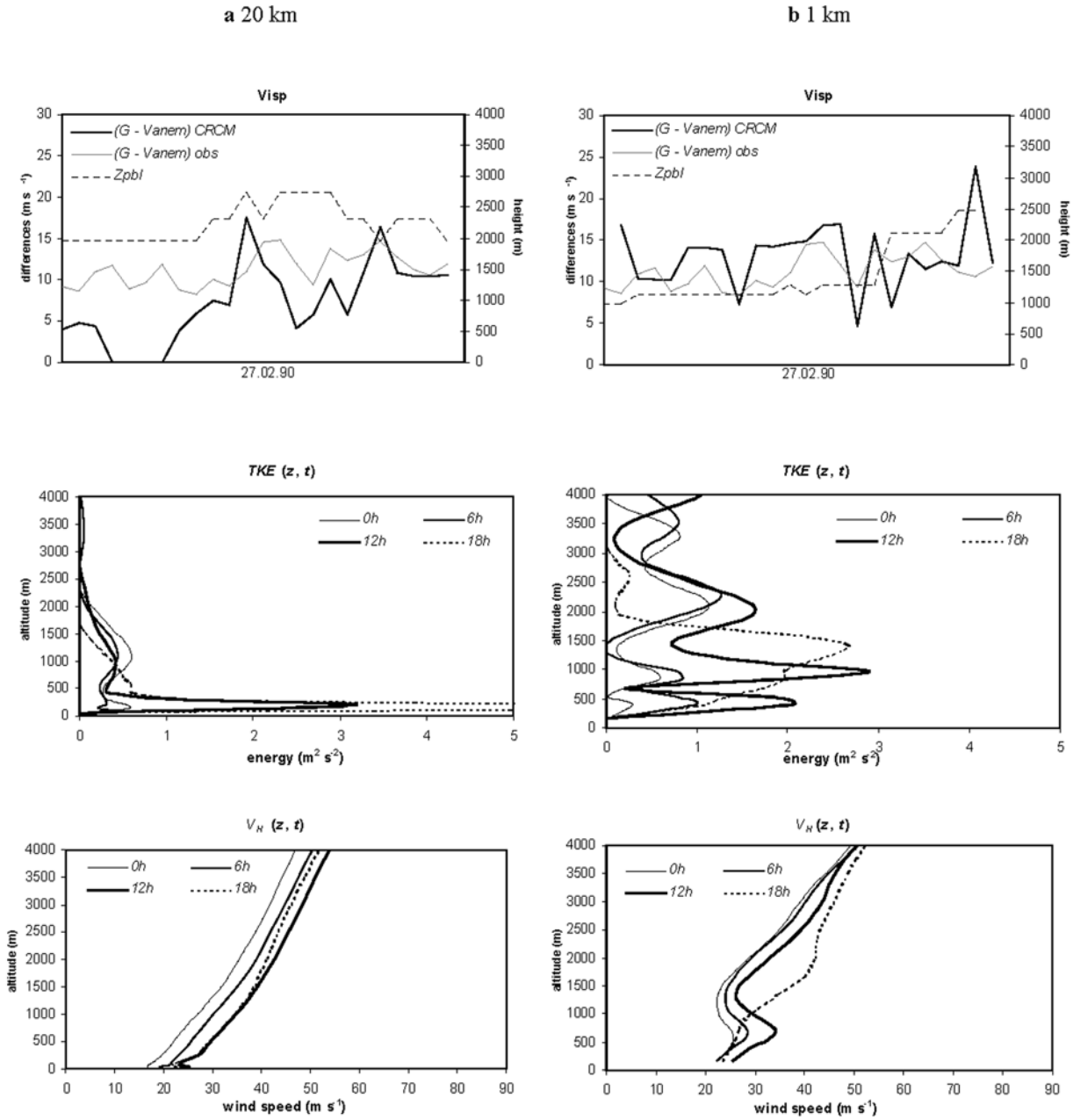

Figure 11. Observed and simulated hourly gusts and hourly mean wind speed differences $\overline{G} - \overline{V}_{anem}$ (m s^{-1}), simulated PBL height (m), TKE and wind profiles, $V_H(z, t)$, at 0, 6, 12, and 18 hours UTC, at station Visp (Switzerland) during the VIVIAN storm with CRCM at 20 km grid spacing (Figure 11a) and 1 km grid spacing (Figure 11b). Vertical axes are the wind speed difference in m s^{-1} and the height above the resolved surface in meters.

as well as the weakening phase of the wind storms, as shown in Figure 5 during the February 1990 VIVIAN in Switzerland and in Figure 10 during December 1999 LOTHAR episode in Belgium, respectively. Finally, a preliminary comparison of daily averages of simulated wind gusts with forest damages during the VIVIAN [*Holenstein*, 1994] and LOTHAR storms in Switzerland (Swiss Forest and Wildlife Department, http://www.fr.ch/sff/forets/lothar.htm, 2002) shows significant correlations, meaning that the spatial location of the simulated strong winds are well captured. In practical terms, these results are particularly interesting at the 1-km CRCM grid spacing.

[59] In this study, the wind gust module is employed as a diagnostic tool using the flow fields simulated by the CRCM. In its current state, the scheme is computationally affordable since it requires an increase of about 2.3% of the original model time spent on a CPU. It may easily be implemented in the numerical model, which solves for the quantities involved in the gust computations, namely the TKE and the buoyant forces in the vertical (see equation

Table 3. Daily Statistics of Observed and Simulated Differences Between Wind Hourly Gusts and Hourly Mean in Switzerland and Belgium For VIVIAN and LOTHAR[a]

Station Name and Number	Grid	$\overline{G}-\overline{V}_{anem}$ Mean, m s^{-1}	$\overline{G}-\overline{V}_{anem}$ Standard Deviation, m s^{-1}
	Switzerland, 27 February 1990		
Jungfraujoch (1)	observed	26.7	4.1
	20	5.9	4.1
	5	11.8	2.3
	1	21.0	6.0
Visp (2)	observed	11.2	2.0
	20	7.2	4.8
	5	16.0	2.6
	1	13.1	3.9
Zermatt (3)	observed	12.3	7.9
	20	6.9	4.7
	5	15.0	2.2
	1	20.0	7.3
	Switzerland, 26 December 1999		
Jungfraujoch (1)	observed	19.7	6.7
	20	6.5	2.5
	5	10.2	2.9
	1	14.1	6.3
Plaffeien (4)	observed	12.4	4.1
	20	6.0	2.5
	5	12.6	3.9
	1	17.5	5.5
Moléson (5)	observed	18.0	5.4
	20	5.5	2.7
	5	10.3	4.0
	1	13.1	7.4
	Belgium, 27 February 1990		
Middelkerke (7)	observed	9.9	3.7
	20	1.8	1.0
	5	8.8	3.7
	1	–	–
Zaventem (8)	observed	10.6	4.7
	20	5.7	5.9
	5	10.3	3.6
	1	9.9	3.5
Saint Hubert (9)	observed	11.8	2.6
	20	3.8	4.1
	5	9.4	2.9
	1	7.5	8.3
	Belgium, 26 December 1999		
Middelkerke (7)	observed	9.2	3.1
	20	1.1	1.6
	5	7.8	4.0
	1	–	–
Zaventem (8)	observed	9.8	1.8
	20	2.5	3.7
	5	6.8	3.5
	1	–	–
Saint Hubert (9)	observed	9.1	2.1
	20	1.8	3.5
	5	9.3	2.2
	1	4.4	5.0

[a]Daily mean is the arithmetical mean of the differences over a complete diurnal cycle, the standard deviation is computed as the root mean square of the average square of the differences about the daily mean.
[b]Numbers in parentheses correspond to those in Figure 1.

(6)). The scheme is thus a potential candidate for implementation in a NWP model.

5. Conclusion

[60] The implementation of a wind gust parameterization in the Canadian regional climate model has been presented in this paper. The wind gust speed is determined with the help of the parameterized effect of turbulence kinetic energy, planetary boundary layer depth, as well as the resolved horizontal wind speed, according to the original ideas of *Brasseur* [2001]. A validation based on two severe wind cases in western Europe has been discussed. Models such as the CRCM have allowed the generation of time series of spatially distributed surface maps of gust speeds, which would not be possible with simpler models. CRCM has shown skill in capturing the spatial and temporal variability of severe wind gusts patterns during two episodes namely the February 1990 VIVIAN and December 1999 LOTHAR.

[61] This method does not consistently reproduce the exact magnitude and variability associated with such small-sized rapidly evolving phenomena at all spatial scales; however, the parameterization is capable of simulating most of the strengthening and the weakening phases of these two storms. The response generally varies as a function of the resolution and the gust speeds are sensitive to the simulation of the model PBL stability. In fact, in most models that attempt to solve for the mean atmospheric state, the similarity theory underlying the parameterization scheme used to represent the atmospheric PBL assumes steady state and equilibrium atmospheric conditions that are rarely the norm during extreme events. In addition, the stable PBLs in Switzerland and in Belgium during the VIVIAN and LOTHAR storms are also difficult to model and (or) to simulate. Furthermore in this study, the wind gust estimates were derived from simulations of PBL wind speeds.

[62] The storm-dependent results are a function of the model configuration during the self-nesting procedure. The gust speeds are highly resolution-dependent: when compared with observations, the simulated gusts are generally more realistic at higher resolution over the complex topography of Switzerland but less sensitive over the relatively flat terrain of Belgium. The model response is highly dependent upon the resolved distribution and height of the terrain: consequently, simple scaling coefficients relating gust speeds with resolutions cannot be easily determined.

[63] It can therefore be concluded that the implementation of this method for computing wind gusts in the CRCM has produced reasonable and valuable results during the VIVIAN and LOTHAR extreme windstorms.

[64] Work is now underway to couple the wind gust with the flow field in the PBL. This will be undertaken by considering the modification of the momentum exchange coefficient, K_m that takes into account the gusty nature of the wind in layers above the surface. Furthermore, this method will also take deep convection into account according to the ideas of *Brasseur* [2001]; this will help to capture a number of additional events that have not been considered in this paper.

[65] **Acknowledgments.** This work has been supported by the Swiss Natural Science Foundation under its network-research initiative "NCCR-Climate."

References

Beljaars, A. C. M., The influence of sampling and filtering on wind gusts, *J. Atmos. Oceanic Technol.*, *6*, 613–626, 1987.

Biner, S., D. Caya, R. Laprise, and L. Spacek, Nesting of RCMs by imposing large scales, in *Research Activities in Atmospheric and Oceanic*

Modelling, No. 987, *Rep. 30*, pp. 7.3–7.4, World Meteorol. Organ., Geneve, 2000.
Blackadar, A. K., The vertical distribution of wind and turbulent exchange in neutral atmosphere, *J. Geophys. Res.*, *67*, 3095–3112, 1962.
Brasseur, O., Development and Application of a Physical Approach to Estimating Wind Gusts, *Mon. Weather Rev.*, *129*, 5–25, 2001.
Brasseur, O., H. Gallée, H. Boyen, and C. Tricot, Reply, *Mon. Weather Rev*, *130*, 1936–1942, 2002.
Burk, S. D., and W. T. Thompson, Comments on "Development and application of a physical approach to estimating wind gusts," *Mon. Weather Rev.*, *130*, 1933–1935, 2002.
Caya, D., and R. Laprise, A semi-implicit semi-Lagrangian regional climate model: The Canadian RCM, *Mon. Weather Rev.*, *127*, 341–362, 1999.
Darling, R. W. R., Estimating probabilities of hurricane wind speeds using a large-scale empirical model, *J. Clim.*, *4*, 1035–1046, 1991.
Davies, F. K., and H. Newstein, The variation of gust factors with mean wind speed and with height, *J. Appl. Meteorol.*, *7*, 372–378, 1968.
Endlich, R. M., and G. S. McLean, Empirical relationships between gust intensity in clean-air turbulence and certain meteorological quantities, *J. Appl. Meteorol.*, *4*, 222–227, 1965.
Goyette, S., M. Beniston, D. Caya, R. Laprise, and P. Jungo, Numerical investigation of an extreme storm with the Canadian Regional Climate Model: The case study of windstorm VIVIAN, Switzerland, February 27, 1990, *Clim. Dyn.*, *18*, 145–168, 2001.
Hart, R. E., and G. S. Forbes, The use of model-generated hourly soundings to forecast mesoscale phenomena: Part II. Initial assessment in forecasting nonconvective strong wind gusts, *Weather Forecasting*, *14*, 461–469, 1999.
Holenstein, B., Dégâts provoqués par la tempête de 1990 dans les forêts en Suisse, OFEFP, Cahier de l'environnement 218, 41 pp., Office Fédéral de l'Environnement, des Forets, et du Paysage, Berne, Switzerland, 1994.
Jagger, T., J. B. Elsner, and X. Niu, A dynamic probability model of hurricane winds in coastal countries of the United States, *J. Appl. Meteorol.*, *40*, 853–863, 2001.
Jungo, P., S. Goyette, and M. Beniston, Daily wind gust speed probabilities over Switzerland according to three types of synoptic circulation, *Int. J. Climatol.*, *22*, 485–499, 2002.
Kalnay, E., et al., The NCEP-NCAR 40-year reanalysis project, *Bull. Am. Meteorol. Soc.*, *77*, 437–471, 1996.
Krayer, W. R., and R. D. Marshall, Gust factors applied to hurricane winds, *Bull. Am. Meteorol. Soc.*, *73*, 613–617, 1992.
Kunkel, K. E., R. A. Pielke Jr., and S. A. Changnon, Temporal fluctuations in weather and climate extremes that cause economic and human health impacts: A review, *Bull. Am. Meteorol. Soc.*, *80*, 1077–1098, 1999.
Laprise, R., D. Caya, G. Bergeron, and M. Giguère, The formulation of the André Robert MC^2 (mesoscale compressible community) model, *Atmos. Ocean*, *35*, 195–220, 1997.
Laprise, R., D. Caya, M. Giguere, G. Bergeron, H. Coté, J.-P. Blanchet, G. J. Boer, and N. A. McFarlane, Climate and climate change in Western Canada as simulated by the Canadian regional climate model, *Atmos. Ocean*, *36*, 119–167, 1998.
McCann, D. W., A simple turbulent kinetic energy equation and aircraft boundary layer turbulence, *Natl. Weather Digest*, *23*, 13–19, 1999.
McFarlane, N. A., and R. Laprise, Parameterization of sub-grid scale processes in the AES/CCC spectral GCM, *Rep. 85-12*, 70 pp., CCRN 17, Can. Clim. Program, Toronto, Ont., Canada, 1985.
McFarlane, N. A., G. J. Boer, J.-P. Blanchet, and M. Lazare, The Canadian climate centre second generation general circulation model and its equilibrium climate, *J. Clim.*, *5*, 1013–1044, 1992.
Meehl, G. A., et al., An introduction to trend in extreme weather and climate events: Observations, socioeconomic impacts, terrestrial ecological impacts, and model projections, *Bull. Am. Meteorol. Soc.*, *81*, 413–416, 2000.
Mellor, G. L., and T. Yamada, A hierarchy of turbulence closure models for planetary boundary layers, *J. Atmos. Sci.*, *31*, 1791–1806, 1974.
Mellor, G. L., and T. Yamada, Development of a turbulent closure model for geophysical fluid problems, *Rev. Geophys.*, *20*, 851–875, 1982.
Mitsuta, Y., and O. Tsukamoto, Studies on spatial structure of wind gust, *J. Appl. Meteorol.*, *28*, 1155–1161, 1989.
Moeng, C.-H., and P. P. Sullivan, A comparison of shear- and buoyancy-driven planetary boundary layer flows, *J. Atmos. Sci.*, *51*, 999–1022, 1994.
Palutikof, J. P., B. B. Brabson, D. H. Lister, and S. T. Adcock, A review of methods to calculate extreme wind speeds, *Meteorol. Appl.*, *6*, 119–132, 1999.
Schüepp, M., H. H. Schiesser, H. Huntrieser, H. U. Scherrer, and H. Schmidtke, The winterstorm "VIVIAN" of 27 February 1990: About the meteorological development, wind forces and damage situation in the forests of Switzerland, *Theor. Appl. Climatol.*, *49*, 183–200, 1994.
Stull, R. B., *An Introduction to Boundary Layer Meteorology*, 666 pp., Kluwer Acad., Norwell, Mass., 1988.
Swiss Climatological Atlas, edited by the Swiss Institute of Meteorology, *Booklet 2–10*, Office Fédéral de la Topographie, Wabern-Bern, Switzerland, 1995.
Troen, I., and L. Mahrt, A simple model of the boundary layer: Sensitivity to surface evaporation, *Boundary Layer Meteorol.*, *37*, 129–148, 1986.
Vogelezang, D. H. P., and A. A. M. Holtslag, Evaluation and model impacts of alternative boundary-layer height formulations, *Boundary Layer Meteorol.*, *81*, 245–269, 1996.
Weggel, J. R., Maximum daily wind gusts related to mean daily wind speed, *J. Struct. Eng.*, *125*, 465–468, 1999.
Wernli, H., S. Dirren, M. A. Liniger, and M. Zillig, Dynamical aspects of the life-cycle of the winter storm "LOTHAR" (24–26 December 1999), *Q. J. R. Meteorol. Soc.*, *128*, 405–429, 2002.
Zwiers, F. W., and V. V. Kharin, Changes in the extremes of the climate simulated by CCC GCM2 under CO_2 doubling, *J. Clim.*, *11*, 2200–2222, 1998.

M. Beniston and S. Goyette, Department of Geosciences, University of Fribourg, Pérolles, CH-1700 Fribourg, Switzerland. (stephane.goyette@unifr.ch)

O. Brasseur, Laboratoire d'étude des Transferts en Hydrologie et Environnement, Domaine Universitaire, 1023-1025, rue de la Piscine, BP 53, F-38041 Grenoble Cedex 9, France.